

Additive manufacturing of stellite 6 superalloy by direct laser metal deposition – Part 2: Effects of scanning pattern and laser power reduction in different layers

Moradi, M., Hasani, A., Malekshahi Beiranvand, Z. & Ashoori, A.

Author post-print (accepted) deposited by Coventry University's Repository

Original citation & hyperlink:

Moradi, M, Hasani, A, Malekshahi Beiranvand, Z & Ashoori, A 2020, 'Additive manufacturing of stellite 6 superalloy by direct laser metal deposition – Part 2: Effects of scanning pattern and laser power reduction in different layers', Optics and Laser Technology, vol. 131, 106455.

<https://dx.doi.org/10.1016/j.optlastec.2020.106455>

DOI 10.1016/j.optlastec.2020.106455

ISSN 0030-3992

Publisher: Elsevier

NOTICE: this is the author's version of a work that was accepted for publication in Optics and Laser Technology. Changes resulting from the publishing process, such as peer review, editing, corrections, structural formatting, and other quality control mechanisms may not be reflected in this document. Changes may have been made to this work since it was submitted for publication. A definitive version was subsequently published in Optics and Laser Technology, 131, (2020) DOI: 10.1016/j.optlastec.2020.106455

© 2020, Elsevier. Licensed under the Creative Commons Attribution-NonCommercial-NoDerivatives 4.0 International <http://creativecommons.org/licenses/by-nc-nd/4.0/>

Copyright © and Moral Rights are retained by the author(s) and/ or other copyright owners. A copy can be downloaded for personal non-commercial research or study, without prior permission or charge. This item cannot be reproduced or quoted extensively from without first obtaining permission in writing from the copyright holder(s). The content must not be changed in any way or sold commercially in any format or medium without the formal permission of the copyright holders.

This document is the author's post-print version, incorporating any revisions agreed during the peer-review process. Some differences between the published version and this version may remain and you are advised to consult the published version if you wish to cite from it.

Additive Manufacturing of Stellite 6 Superalloy by Direct Laser Metal Deposition – Part 2: Effects of Scanning Pattern and Laser Power Reduction in Different Layers

Mahmoud Moradi^{1,2}, Arman Hasani², Zeinab Malekshahi Beiranvand³, Ali Ashoori^{1,2}

1-Department of Mechanical Engineering, Faculty of Engineering, Malayer University, Malayer, Iran.

2-Laser Materials Processing Research Center, Malayer University, Malayer, Iran.

3- Department of Materials science and Engineering, Tarbiat Modares University, Tehran, Iran.

Abstract:

In this study, the purpose is to investigate two strategies for direct laser metal deposition method (DLMD) additive manufacturing of stellite 6 Cobalt-based superalloy experimentally. The first one was the effect of scanning pattern, and the second one was the influence of laser power reduction in different layers in additive manufacturing (AM). For the experiments a coaxial nozzle head coupled with a 1 kW continuous fiber laser was used. This research aim was to examine the effect of these two strategies on characteristics of the additive manufactured components. The macro section of the geometrical dimensions, including height and width, profiles of microhardness, grain size, and microstructure of the 3D printed wall samples were investigated. The height stability of samples was also examined. The results indicated that scanning pattern has an important role in all the additive manufactured components features. Results show that when the unidirectional scanning pattern was used, the more stability will be obtained. The average grain size of samples which were produced by unidirectional scanning pattern and bidirectional scanning pattern was $2.25 \mu m$ and $2.83 \mu m$, respectively. The trend of changes in the grain size of the samples shows that the beginning and the end of the LAMed wall are larger than the sample's center, and the trend of the microhardness variation is in reverse regime of the grain size. Also, it was shown that with decreasing the laser power from the substrate upwards, the width of samples has reduced.

Keywords: Additive Manufacturing; Direct Laser Metal Deposition; Scanning pattern; Dimensional Stability; Grain size; Hardness.

1. Introduction

Additive manufacturing (AM) is an efficient way of producing components compared with the conventional subtractive manufacturing process. It has been profoundly used in aerospace applications from the beginning, and it has rapidly become a new strategic technology for the design and production of high-performance components for aerospace, medical, energy and automotive applications [1-4]. In recent years, 3D printing technology were used to build complex structures and composites. AM processes build 3D printed by progressively adding thin layers of materials guided by a digital model without the need for expensive tooling, forms, or assemble multiple components [3]. AM is made up of various categories and processes. Among these categories, three are laser-based AM processes. Direct laser metal deposition (DLMD), as one of laser-based additive manufacturing methods, uses a coaxial laser beam as the heat source to melt a metallic material in the form of wire or powder, which is supported by the shielding gas, into the melt pool. After the molten metal cools down and solidifies, another layer of material is deposited on top of the solidified layer. Therefore, a fully dense 3D product can be manufactured layer by layer from a Computer-Aided Design (CAD) model [5-9]. The schematic diagram of the direct laser metal deposition process is shown in Figure 1.

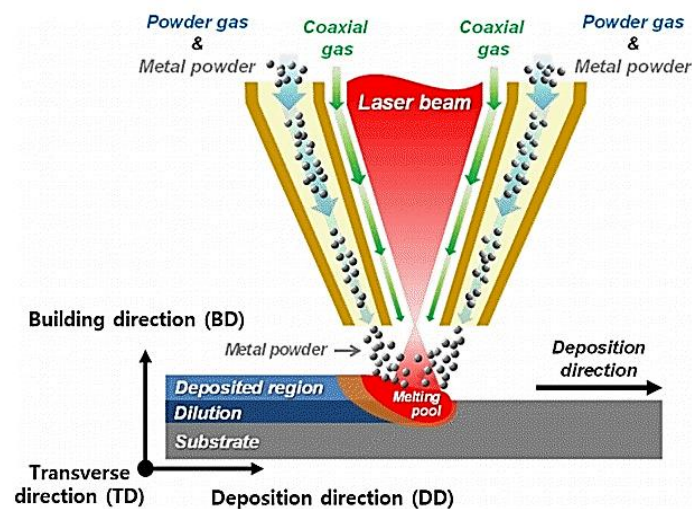


Figure 1: Schematic of the direct laser metal deposition [10].

Many studies in Direct Laser Metal Deposition (DLMD) were carried out using different metal powders such as Inconel, Stellite, Stainless Steels, Aluminum alloys, Titanium alloys, etc. to produce parts by DLMD [11, 12]. Co-Cr-based alloys have widely used as the added material to improve the surface properties of substrate in aerospace, marine, automotive, petrochemical, and medical application due to their excellent properties such as high strength, wear/corrosion resistance and hardness [4,

6]. Various kinds of cobalt-based alloys called ‘stellite’ have been used in fields requiring high heat and corrosion resistance and high wear strength. This alloy is ideally suited to a variety of hard facing processes [13]. Applications, as well as properties of Stellite alloys, are widely determined by their chemical compositions [4]. Alloying elements such as Cr, W, and Mo contribute to strengthening Co-Cr-based alloys with the formation of a solid solution matrix [4]. Stellite 6 was the first Stellite alloy developed in the early 1900s [4]. Traditional processing methods for part production of Stellite alloys, including casting, forging, milling, and hot isostatic pressing has a lot of defects [4, 6]. Also, due to the presence of tungsten, it is intrinsically difficult and expensive to machining this alloy [4]. Despite the widespread applications of these alloys, an understanding of transport phenomena and solidification behavior in the melt pool still is a challenge [6].

Foster et al. [14] used the DLMD method to repair and to remanufacture of cobalt-based stellite 21 forging dies. They found that the stellite 21 DLMD additive layer has better wear resistance properties than H13 tools steel dies. Characteristics of a material microstructure such as grain size, grain shape, grain orientation, track geometry, mechanical properties, surface roughness, and microstructure are complex functions of process parameters. Direct Laser Metal Deposition (DLMD) is a new complex process involving a large number of parameters that can be effective on the final characteristics of a manufactured part [15]. Scanning speed, beam power, scanning strategy, hatch distance (scan-line spacing), and thickness of the powder layer are considered as the principal parameters in Laser AM [16- 20]. It is mentioned that several authors have attempted to make the relation between final characteristics and process variables via analytical, numerical, or experimental means [18]. Caiazzo et al. compared the effects of unidirectional laser scanning deposition and bidirectional scanning deposition on the forming properties of LMD Al 2024 [16]. It was shown that the deposition pattern played a significant role in the evolution of microstructural and grains direction [16]. The effects of temperature gradients and the shape of the molten pool on the morphology and orientation of the microstructure were discussed under two different deposition patterns [16].

Notwithstanding the great efforts by so many researchers, various aspects related to direct laser metal deposition additive manufacturing of super alloys are still unsolved and much more research should be done with the aim of analyzing the possible benefits arising from DLMD process, a new concept for manufacturing and repairing. This is not a simple task because of the large number of process parameters. Within this context, considering different scanning pattern and laser power reduction in

different layers of AM samples, and investigating the geometrical stability of the additively manufactured walls, are relatively new additions to this field. In the present research, stellite 6 Cobalt-based superalloy powder was used for 3D printing via a direct laser metal deposition method. The capabilities of the additive manufacturing were investigated by two strategies: (1) changing the scanning pattern (unidirectional and bidirectional scanning pattern) (2) variation and reduction of the laser power in any scanning pattern. The macro section of the geometrical dimensions (height and width), microhardness profile, grain size, and the microstructure of the 3D printed samples were characterized. The geometrical stability of the printed wall of the manufactured sample is another novelty aspect of this investigation. Some microstructural control has also been demonstrated in laser additive manufacturing by varying laser power and varying scan strategies.

2. Experimental Work

2-1. Materials

In this study, Cobalt-base super-alloy stellite 6 powder with a particle size of 10 to 36 micrometers was used. The substrate was DIN 1.2714 hot work tool steel (56NiCrMoV7). Table 1 shows the chemical composition of the powder and the substrate, identified by the X-ray fluorescence spectrometer (XRF) model PW1410. The moderate carbon of the substrate steel, chrome, nickel, and molybdenum caused high impact and fatigue strength in high temperature and thermal shock and wear resistance. The substrates were prepared by machining in dimensions of 80×20 mm with a thickness of 7 mm. The surfaces of the samples were grounded. Figure 2 depicts the morphology of the powder particles taken by scanning electron microscopy (SEM 3MIRA).

Table 1: Chemical composition of the stellite 6 powder and DIN 1.2714 substrate

Element	Co	Cr	W	Fe	P	Mn	C	Si	S	Ni	Mo
Powder (wt. %)	Bal.	31	3	1.21	0.42	0.22	1.3	-	-	-	-
Substrate (wt. %)	-	1-1.2	-	Bal.	0.03	0.6-0.9	0.5-0.6	0.1-0.4	0.03	1.5-1.8	0.45-0.55

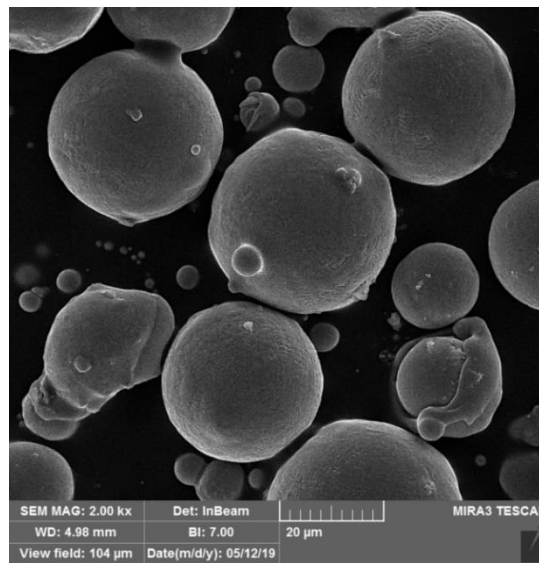


Figure 2: SEM image of stellite 6 powder particles

2-2. Direct Laser Metal Deposition Process (DLMD)

Considering the desired condition of the powder stream, the DLMD additive manufacturing process was carried out. For the DLMD process, a 1 kW Fiber laser (YFL-1000 model made in Iranian National Laser Center) with the minimum spot size of the laser at the focal position of 0.2 mm, the focal length of 200 mm, and the Rayleigh length of 2 mm was operated in a continuous wave. Cobalt-base super-alloy stellite 6 powder was deposited on the DIN1.2714 hot work tool steel substrate.

A dense powder stream was needed for a DLMD additive manufacturing process, so a brass nozzle with four annular channels was designed to focus the powder particles in the powder concentration plane (Figure 3) [21]. Different parameters such as powder flow rate, the axial and annular carrier argon shielding gases flow rate, and standoff distance varied. In the best setting (coaxial gas flow rate = 3 lit/min and annular gas flow rate = 6 lit/min), as shown in Figure 3. The concentration zone of the powder

stream was recognized 15 mm under the powder coaxial nozzle. In this powder set, the powder flow rate was measured equal to 20 g/min. Laser additive manufacturing experimental works were performed in four strategies, as presented in Table 2.

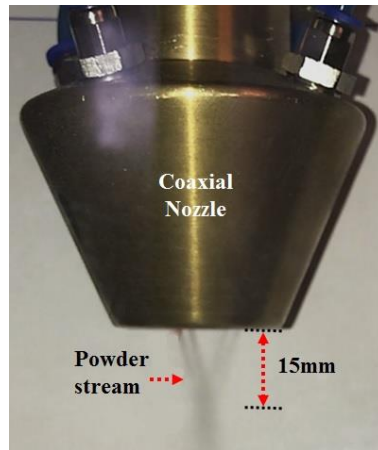


Figure 2: Powder stream and its concentration under the coaxial nozzle [21].

Table 1: Concept of applied strategies in the research

	Sample name	Scanning pattern	Laser power (W)
Strategies	D1	Unidirectional ⇒	250
	D2	Bidirectional ⇔	250
	P1	Unidirectional ⇒	300-100
	P2	Bidirectional ⇔	300-100

In all experiments, the scanning speed, standoff distance, and the powder flow rate were kept fixed 10 mm/s, 15 mm, and 20 g/min, respectively. In all samples, after adding each layer, the CNC table moves 0.3 mm down for adding the next layer on the previous manufactured layer. Figure 4 illustrates a schematic of the additive manufactured deposited layers on the substrate. For the investigation of Geometrical dimensions, width (w) and height (h) of the deposited wall, depth of the penetration of the layer in the substrate (d_1), and depth of the HAZ area (d_2) were measured.

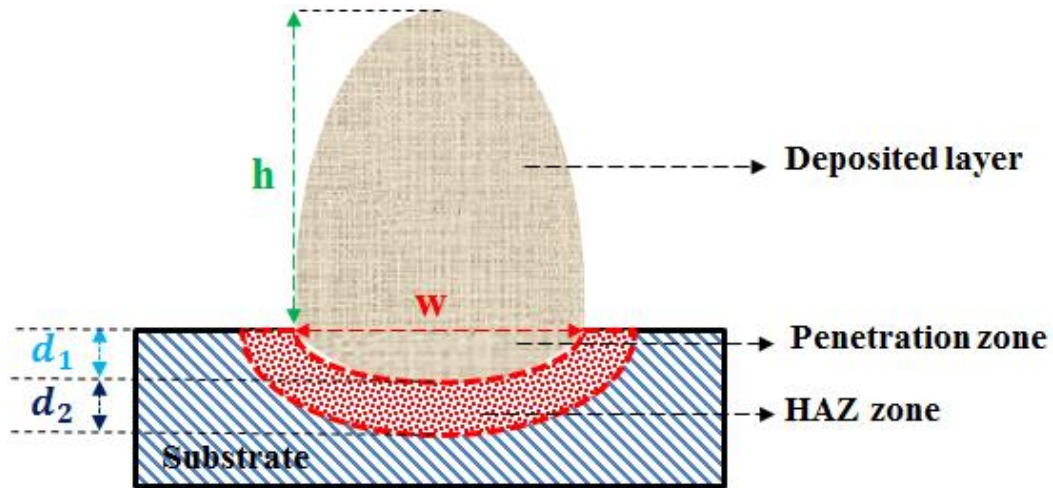


Figure 3: A schematic of the additive manufactures deposited layers on the substrate.

2-3. Characterizations

The Laser Additive Manufactured (LAMed) samples were cut from the middle, and the cut specimens mounted in resin. Samples were polished, and then for microstructure analysis and metallographic investigations, the samples have been etched. The reagent with a formula of 90 ml of HCl, 7 ml of H₂SO₄ and, 3 ml of 3HNO₃ was used. OM and SEM images are taken by Kayowa optical microscope and scanning electron microscope (model LEO1455VP). Microhardness tests were performed by using the NEXUS 4000 microhardness according to the Vickers standard along with the height of the LAMed wall with a load of 500 g and dwell time of 15 seconds. Image j software version 1.32J, was used to analyze the geometric dimensions, grains size measurements, and geometric stability of the LAMed wall.

3. Results and Discussion

In this study, the effect of scanning pattern on the geometrical dimensions, wall height stability, grain size, and microhardness in fiber laser additive manufacturing process of stellite 6 powder with the 1.2714 steel substrate was investigated.

3.1 Surface quality of additive manufactured samples

Figure 5 shows the laser additive manufactured (LAMed) wall with different strategies. In D series samples, the first and second strategies (Figure 5), constant power of 250 Watts, is used. That they were made in unidirectional scanning with 50

seconds cooling time between layers (D1) and bidirectional scanning with 35 seconds cooling time between layers (D2), respectively. In the first strategy, the unidirectional sample (D1), the scan only went in motion without any reversal. When each layer was formed, the laser head is placed at the beginning of the previously formed layer and created another layer on it. Also, for each sample the entire each created layer is uniformly cooled at equal time intervals. This causes the sample to have lower distortion and better surface quality than the bidirectional sample (D2) after the layers are formed.

In P series, the third and fourth strategies (Figure 5), two scanning patterns with different laser power (from 300 to 100 W) in each layer applied. The first layer starts at 300 W and ends at the fifth layer at 100 W. Each layer is fabricated by a 50 W power reduction from the previous one. In the third strategy, scanning was performed unidirectional, with a cooling time of 50 seconds between layers (P1), in the fourth strategy, scanning was performed bidirectional, with a cooling time of 35 seconds between layers (P2).

After fabricating these two samples, it was found that due to the decrease in power from the first layer to the up layer, each layer has less width and thickness than the previous one. And finally, the wall created from beginning to end on the substrate forms a cone- shaped. Also, sample P1 due to unidirectional scanning has less distortion and more desirable surface quality than sample P2 (See Figure 6).

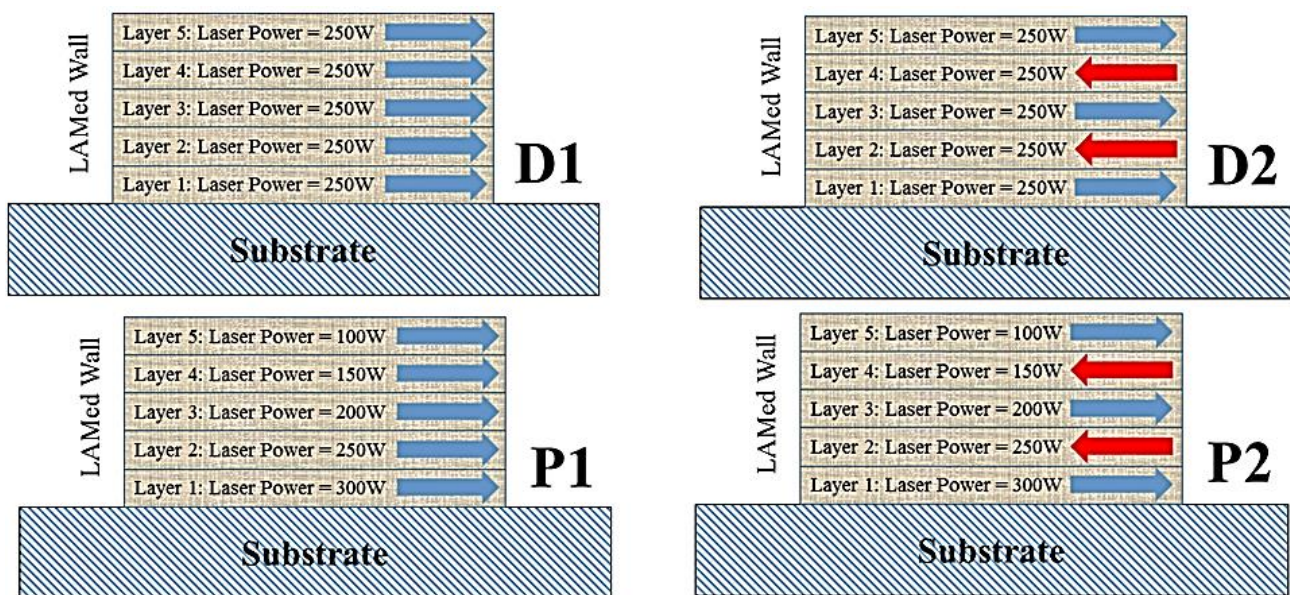


Figure 4: The scanning pattern of the Laser Additive Manufactured samples (LAMed Wall)

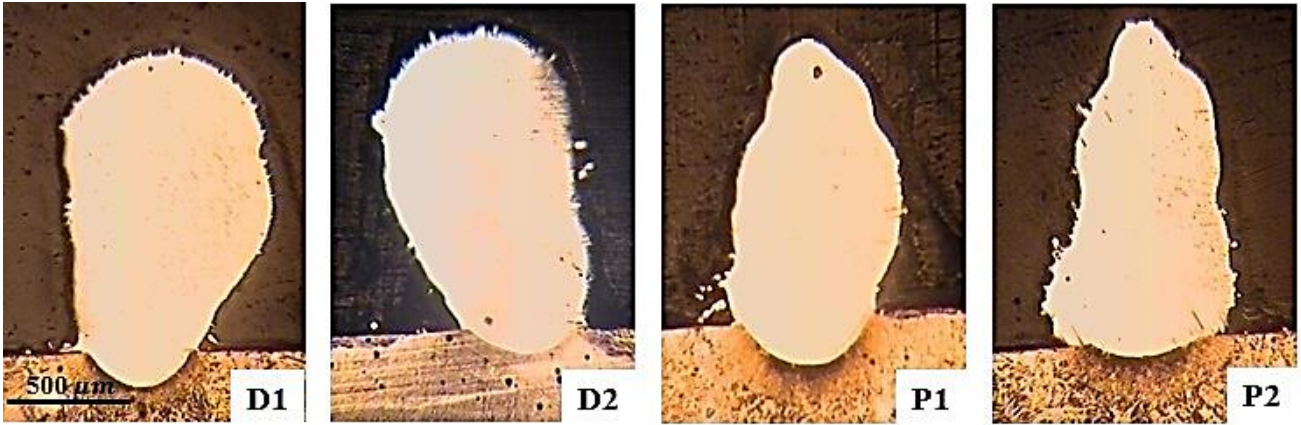


Figure 5: Macro section of laser additive manufactured samples.

3-2. Additive Manufactured Case Geometry

The results of the geometrical dimensions' measurements presented in Figure 7 and Table 3 for all samples. Figure 8 depicts the LAMed samples.

Table 2: Geometrical dimensions results of Additive Manufactured samples.

Sample name	w(μm)	h(μm)	d ₁ (μm)	d ₂ (μm)
D1	527 \pm 30	1245 \pm 30	150 \pm 5	135 \pm 5
D2	507 \pm 25	1160 \pm 28	100 \pm 5	130 \pm 5
P1	607 \pm 55	1150 \pm 55	187 \pm 9	165 \pm 9
P2	635 \pm 50	1320 \pm 52	75 \pm 5	190 \pm 7

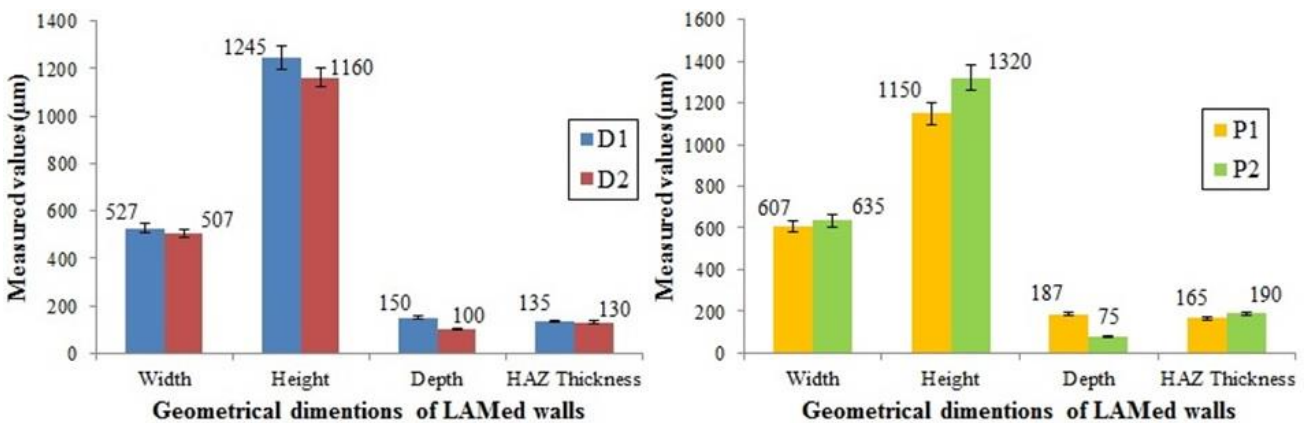


Figure 6: The curves of geometrical dimensions of samples: width, height, depth of penetration in the substrate, and HAZ thickness.



Figure 7: The images of the LAMed samples (the thickness of the substrate is 7 mm).

- **Influence of the scanning pattern on dimensions of D1 and D2 samples (unidirectional and bidirectional, respectively, at constant power):**

Since during LMDS process, the metal part is manufactured by moving a laser source for melting the fed powder and scan all areas of the part on a substrate, layer by layer, the arrangement of scanning pattern, plays a significant role in improving the precision and performance of the produced sample, due to changing the thermal history of each layer [22, 23]. Two samples of D1 and D2 differ only in the scanning direction and cooling time, and other process parameters are kept the same. Samples D1 and D2 were fabricated with a unidirectional and bidirectional scanning patterns, respectively. The cooling time between layers in sample D1 and D2 is 50 seconds and 35 seconds, respectively. Since in sample D1, manufactured by unidirectional scanning, the laser head is restored to the beginning of the previous layer, the created layer at any time cools uniformly. It also takes a longer time to cool the sample. Increasing the cooling time causes the formed layer on the substrate to have better surface quality. So, sample D1 has better surface quality than the sample D2. Also, the D1 sample is geometrically more significant than the D2 in terms of width, height, depth penetration in the substrate, and HAZ area. But the difference between depth penetrations in the substrate in two samples is pronounced. In the unidirectional pattern (D1), the next layers always deposited on the layer with less temperature and as a result with a high thermal gradient. In comparison, in the bidirectional pattern (D2) the temperature of the previous layer is higher and as a result, the thermal gradient is lower. The deposition pattern is effective on the temperature gradient and the shape of the molten pool [18]. In samples produced by unidirectional scanning (D1) in comparison to samples produced by bidirectional scanning (D2), increasing the thermal gradient within each layer increases residual stresses and therefore decreases heat distortion [24]. Furthermore, the D1 sample, in comparison D2 sample, experiences higher interval times between layers that lead to higher cooling rate, leading to a finer microstructure and higher tensile strength and, as a result, lower distortion [25]. It was

shown that with decreasing the enter-layer time intervals, the bulk heating effects would increase. So, the cooling rates of the subsequent layer were affected by the initial temperature of the previously deposited layer [25].

- **Effect of the scanning pattern on dimensions of P1 and P2 Samples (unidirectional and bidirectional, respectively, with decreasing power from the first to the end layer)**

These two samples differ only in the laser scanning direction and cooling time. The sample P1 and P2 were fabricated with unidirectional and bidirectional scanning patterns, respectively. The other process parameters are the same. In both samples, the first layer was deposited by the laser power of 300 W, and the fifth layer was finished using the power of 100 W. In fact, each layer is fabricated by a 50 W power reduction from the previous one. Five layers were deposited on each other. The cooling time between layers in sample P1 and P2 is 50 seconds and 35 seconds, respectively. Since sample P1 was fabricated by a unidirectional scanning pattern, the layer created at any time is uniformly cooled. It is also cooled in a longer time. Increasing the cooling time causes the created layer to have a lower heat distortion and a better surface quality. Therefore, it can be said that sample P1 has lower distortion and higher surface quality than sample P2. By comparing these two samples, it can be seen that the geometry of sample P1 is smaller in width, height, and HAZ than in P2 but penetrates deeper into the substrate. In general, the width of these two samples has decreased from the substrate upwards due to the power reduction in each layer. The aim of AM is to achieve the highest and widest sample with the least amount of time, and powder consumption, to reduce production costs, and the penetration depth is not a critical parameter in AM processes.

In the unidirectional pattern (P1) in comparison to the bidirectional pattern (P2), the next layers always deposited on the layer with less temperature and as a result with a high thermal gradient. Furthermore, P1, in comparison to P2, experiences higher interval times between layers, leading to higher cooling rate, and as a result, finer microstructure, higher tensile strength, and finally lower thermal distortion [25]. Since in sample P2 in comparison to P1, inter-layer successive deposition was applied, and the interval between layers is lower, the effect of thermal accumulation would increase with the increased deposited layer [25]. Therefore, the height of the P2 sample is larger than the P1 sample.

3-3. Height Stability of the additively manufactured samples

In the LAM process, one of the important aspects is to have less height variation, smoother LAMed wall, higher surface quality, and less distortion. This means more stability of the LAMed wall. To investigate the stability of the LAMed wall, a photo of the LAMed wall appearance in height was prepared for each LAMed sample, as shown in Figure 9. To determine the wall height stability, the highest and lowest part of the LAMed wall were measured at three regions, including the beginning, middle, and end of the sample, as shown in Figure 9. The absolute height difference shows the variation of the wall height, and as a result of the amount of height stability, i.e., lower difference, means higher stability. In Table 4, h_1 , h_3 , and h_5 are the minimum heights and h_2 , h_4 , and h_6 are maximum heights of the LAMed wall in three regions. Equations 2, 3, and 4 present the wall variation values Δh_1 , Δh_2 , and Δh_3 , respectively:

$$\Delta h_1 = h_2 - h_1 \quad (2)$$

$$\Delta h_2 = h_4 - h_3 \quad (3)$$

$$\Delta h_3 = h_6 - h_5 \quad (4)$$

The instability level for each sample (the higher Δh , the more instability of the wall) is presented by the largest value of three values:

$$\Delta H = \text{Max} \{ \Delta h_1, \Delta h_2, \Delta h_3 \} \quad (5)$$

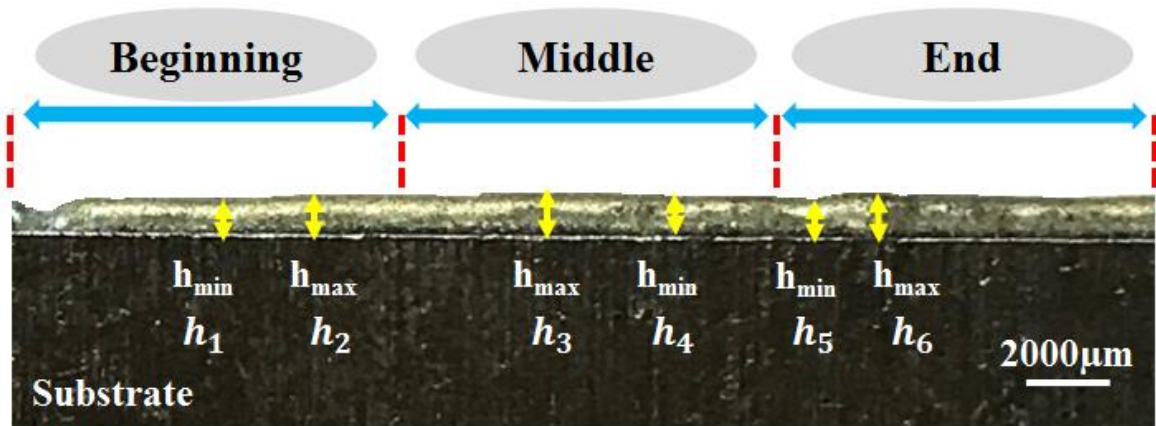


Figure 8: Additive manufactured wall height appearance and the definition of stability through three region height variation.

Table 3: Maximum and minimum of height and differences of them in three regions (beginning, middle, and end of samples).

Sample Number	h_1 (μm)	h_2 (μm)	Δh_1 (μm)	h_3 (μm)	h_4 (μm)	Δh_2 (μm)	h_5 (μm)	h_6 (μm)	Δh_3 (μm)	ΔH (μm)
D1	1103 \pm 3	1152 \pm 3	49 \pm 3	1276 \pm 3	1345 \pm 3	69 \pm 3	1207 \pm 3	1276 \pm 3	69 \pm 3	69 \pm 3
D2	1000 \pm 3	1125 \pm 3	125 \pm 3	1150 \pm 3	1175 \pm 3	25 \pm 3	1150 \pm 3	1383 \pm 3	233 \pm 3	233 \pm 3
P1	1069 \pm 3	1121 \pm 3	52 \pm 3	1138 \pm 3	1241 \pm 3	103 \pm 3	1328 \pm 3	1422 \pm 3	94 \pm 3	103 \pm 3
P2	1008 \pm 3	1221 \pm 3	213 \pm 3	1313 \pm 3	1389 \pm 3	76 \pm 3	1206 \pm 3	1267 \pm 3	61 \pm 3	213 \pm 3

- Effect of the scanning pattern on height stability:

According to Table 4, the largest and the smallest height and their difference in all three regions (beginning, middle, and end of the sample) were calculated for samples D1 and P1 (unidirectional scanning pattern) and D2 and P2 (bidirectional scanning pattern). From the calculated differences in each sample, the largest difference (ΔH) was obtained. This value was 102.9 and 51.8 for sample D2 and D1, respectively. This value was also 103.5 and 213.8 for sample P1 and P2, respectively. The lower the difference, the height stability is more. So, the height stability for D1 is more than D2 and also for P1 is more than P2. Therefore, it can be said scanning direction will also affect on sample stability geometrically. It can be stated that in unidirectional scanning pattern in sample D1 than D2 and P1 than P2, cooling is done more uniformly and appropriately. And it also takes a longer time to cool the sample. Increasing the cooling time makes the layer less distorted, and the surface quality more desirable. For this reason, sample D1 has more height stability than sample D2, and sample P1 has more height stability than sample P2. Figure 9, also shows the variation of maximum height differences calculated by equation 5 (ΔH) for samples, based on the values presented in Table 4. As mentioned before, in this definition, in this paper, the lower the (ΔH) causes the higher stability of the specimen [25, 26]. It is shown in Figure 10 that in samples manufactured by unidirectional scanning pattern, the ΔH and as a result of stability is less than in samples manufactured by bidirectional scanning pattern. Thus, as shown in Figure 10, sample D1 has less ΔH than sample D2, and sample P1 also has less ΔH than sample P2. It is also shown that in the D1 sample, the

less ΔH happen, which means more stability, better appearance, better surface quality, and less distortion. D1 has manufactured using a unidirectional scanning pattern compared with D2. So, in the D1, each created layer cools more uniformly, and as a result, more stability than D2. Also, D1 has manufactured at constant power laser compared with P1 and P2 that have manufactured at variant power.

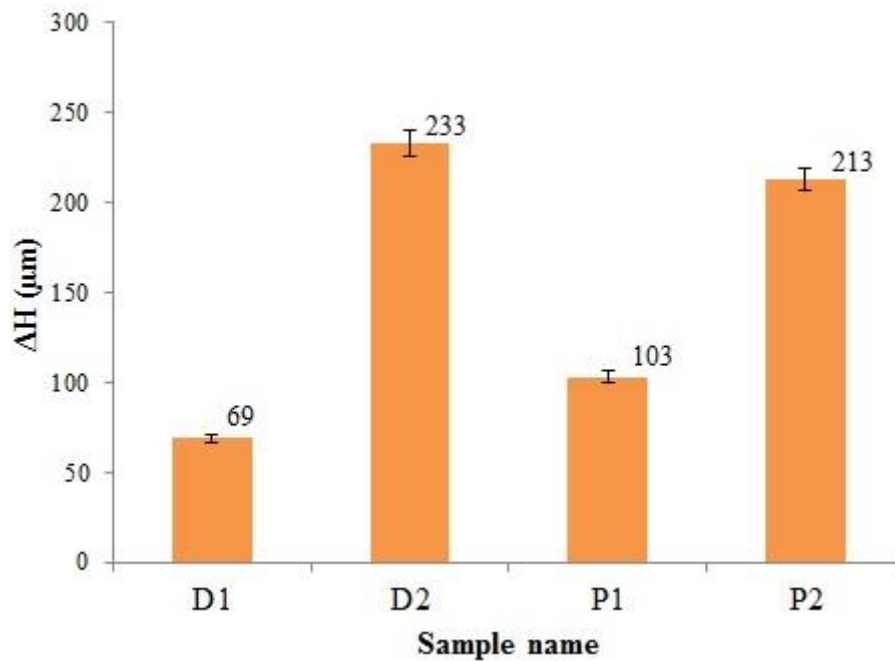


Figure 9: Maximum difference between height (ΔH) for samples.

3-4. Grain size

The grain size was measured using the Heyn method [27]. According to this method, in metallographic images taken by optical microscope from the manufactured samples, some line sections were drawn horizontally, vertically, and diagonally in five different regions, from the beginning, center, and the end of the samples. The number of grains located under each line section was divided by the length of the line section. Finally, by interpolating the grain size in these five regions, the grain size in each sample was obtained in three zones, including beginning (a1 and a2), center (a3 and a4), and end (a5 and a6) of the sample, see Table 5 and Figure 11. Figure 12, shows the optical images of the LAMed samples that were used to apply the Heyn method for measuring the grain size.

Table 4: Grain size values in three areas: beginning, center, and end of Sample

Sample name	a ₁ (μm)	a ₂ (μm)	a ₃ (μm)	a ₄ (μm)	a ₅ (μm)	a ₆ (μm)	Average Grain Size
<i>D</i> ₁	2.6±0.1	2.3±0.1	1.9±0.2	2±0.2	2.3±0.1	2.4±0.1	2.2±0.1
<i>D</i> ₂	3.2±0.1	2.9±0.1	2.2±0.2	2.4±0.2	2.9±0.1	3.4±0.1	2.8±0.2
<i>P</i> ₁	2.7±0.1	2.5±0.1	2.2±0.1	2.1±0.2	1.7±0.2	1.6±0.2	2.1±0.1
<i>P</i> ₂	3.1±0.1	2.8±0.1	2.4±0.1	2.1±0.2	2±0.2	1.8±0.2	2.4±0.1

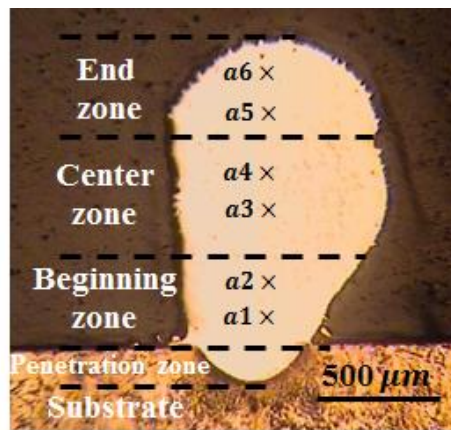


Figure 10: Grain size measured points in different sections (zones) in the LAMed samples.

In addition to what was explained before, it is necessary to mention that, in the DLMD process, when the laser beam interacted with powder particles in the powder stream, the powder particles absorbed the laser beam energy and the laser energy attenuates. It means that the laser energy decreased little by absorbing with different powder particles in the powder stream. Thus, a part of the laser beam energy interacts with the substrate surface, and this leads to melting the substrate if the laser energy is enough. Otherwise, it does not melt the substrate. In the second layer and other layers, it is the same. A part of the laser that does not absorb by the powder stream can melt the previous layer in which the new layer is deposited. So, it is the main explanation of the process that leads to the melted zone in the surface and the interlayer zone in which the powder is deposited. This process caused the fluctuated changes in the microstructure and grain size of those re-melted and recrystallized zones.

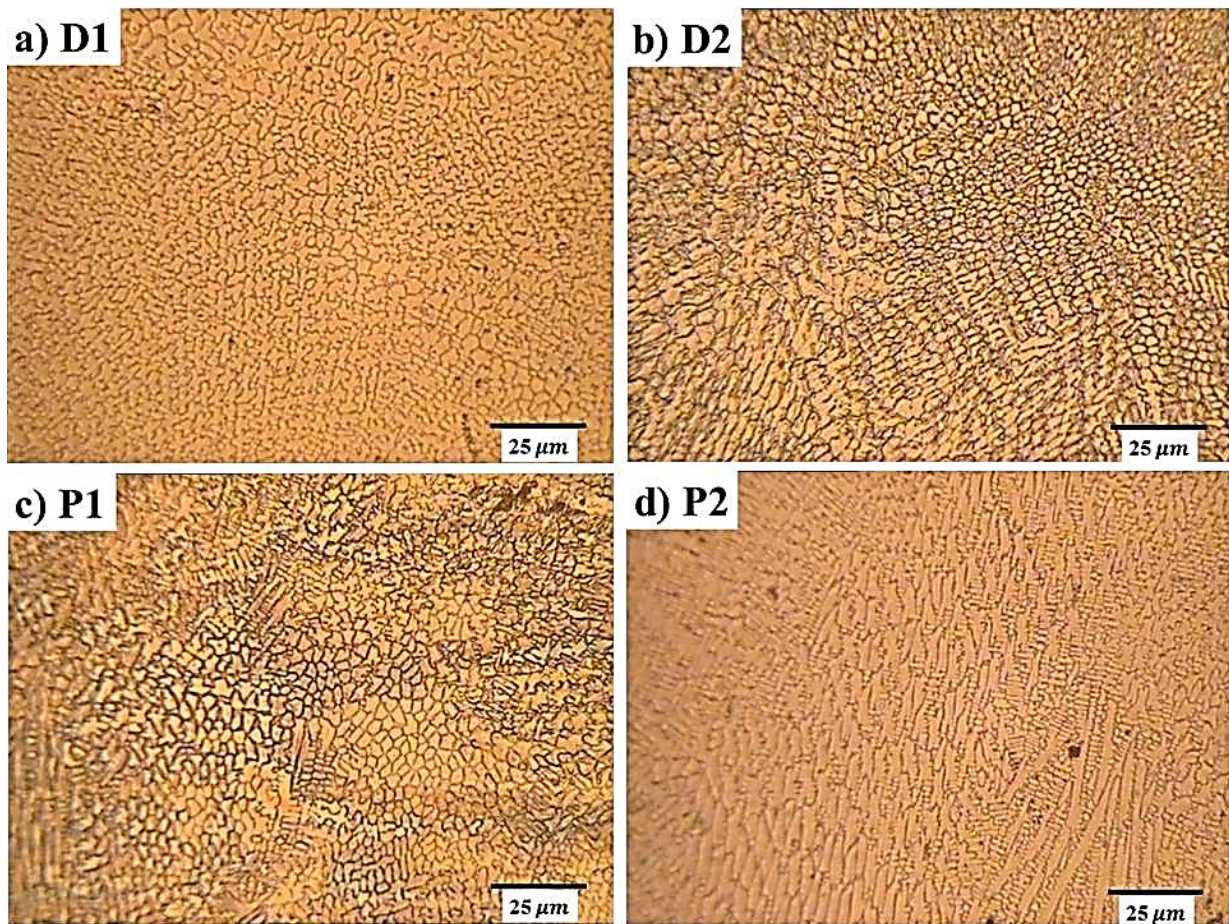


Figure 11: Optical microscopic images of the LAMed samples.

Figure 13 shows the SEM images of the grain size variations in different regions of the LAMed samples. Upper and lower pictures of Figure 13 are grain size images of D1, D2, P1, and P2 samples at the beginning, center, and end of samples, respectively. All series samples have the same trend in grain size, as shown in Figure 14. Figure 14 depicts the trend diagram of the grain size variations in the beginning, center and end of D1, D2, P1, and P2 samples. Since samples P1, P2, D1, and D2 can't absolutely avoid thermal accumulation, and thus, the microstructure size to different regions are different [25].

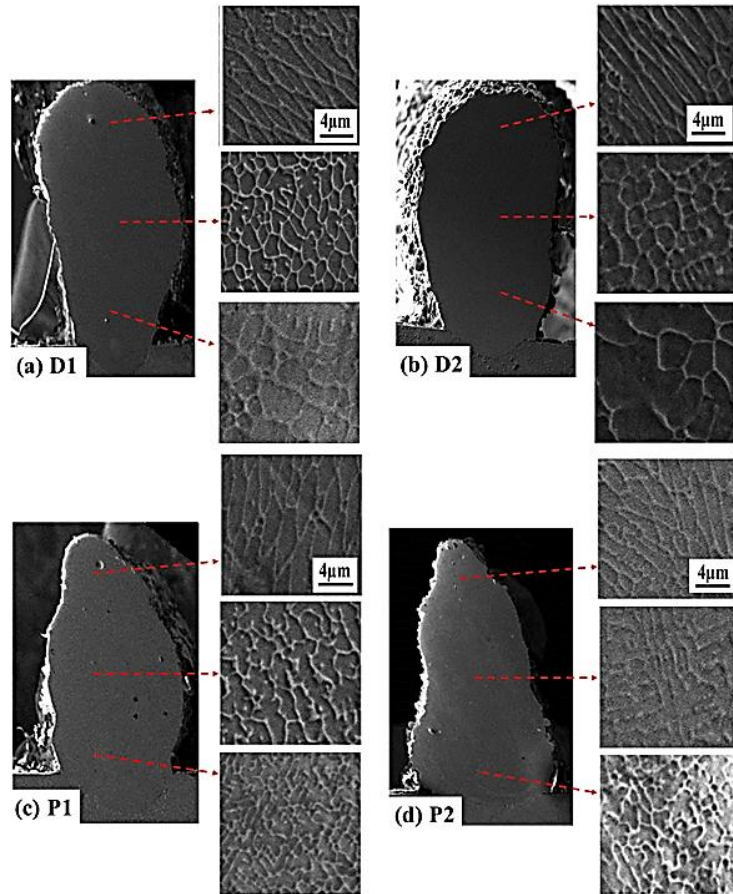


Figure 12: SEM images of grain size changes at the beginning, center, and the end of Sample (a) D1, (b) D2, (c) P1, and (d) P2.

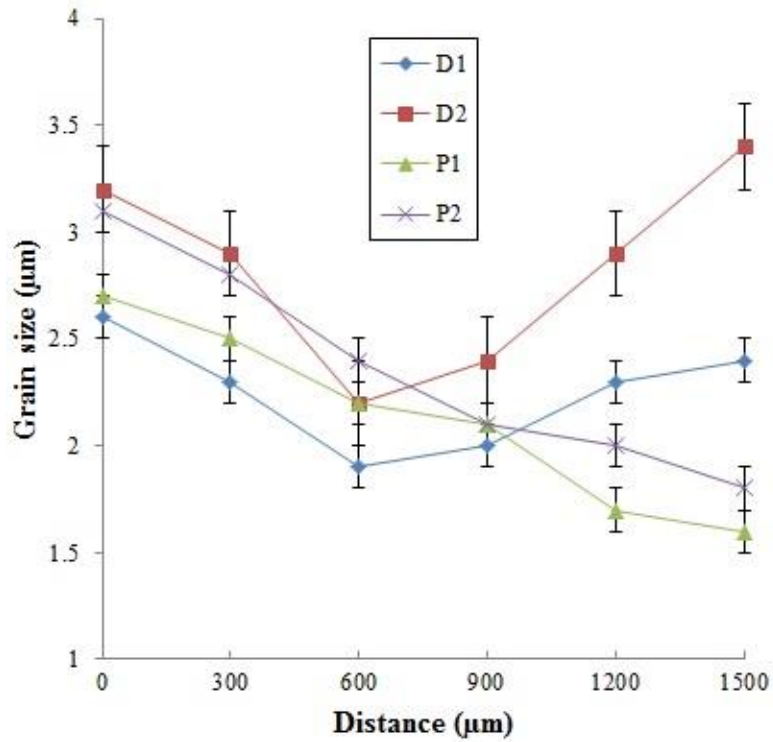


Figure 13: Grain size change trend diagram in D1, D2, P1, and P2 samples.

- Effect of the scanning pattern on the grain size of samples D1 and D2:

Samples D1 (Figure 13a) and D2 (Figure 13b) were fabricated with a unidirectional and bidirectional scanning patterns, respectively. By comparing the grain size in three zones, including the beginning, center, and the end of these samples, it was found that the two samples have similar trends in grain size variations in these three zones. But the values of grain size in these three zones have less difference in sample D1 than in sample D2. The reason for this smaller difference in the grain size of the D1 is that in a unidirectional scanning pattern, the cooling is performed more uniformly throughout the sample, and more time is spent cooling the D1 sample. Increasing the cooling time causes the temperature in the sample to be lower throughout the work cycle, and thus, to reduce the grain size in the whole sample. As a result, sample D1 has a more regular cooling rate because it has a unidirectional scanning direction and longer cooling time. This causes the sample D1 to have a lower temperature during manufacture. Finally, the grain growth is less, and the grains are smaller than sample D2.

The grain size difference in these two samples is confirmed by the SEM images shown above. The SEM image of grain size variations at the beginning, center and end of samples D1 and D2 is shown in Figure 13a and b. The trend of grain size variations for samples D1 and D2 is shown in Figure 14. According to the graphs, it is clear that the grain size has been decreasing from the beginning to the center of the sample and has been increasing from the center to the end of the sample. The grain size at the beginning of the sample is much larger, because the substrate acts as a heat source [29, 30]. When the irradiation of the laser beam occurs, the substrate stored the heat on itself. Because the thermal conductivity of the steel substrate ($k=24.6 \text{ W/m.k}$) is higher than that of stellite 6 ($k=14.82 \text{ W/m.k}$) [29], it transfers this heat to its upper layer. When the next layers deposited (center zone of the sample), the heat conduction from the substrate decreased, so the grain size decreased. The top layers have a larger grain size. In addition to what has been said before, the top of the LAMed layers was conducted with shielding gas and air from one side. These gases have a low heat conduction coefficient, so the absorbed heat in the end layers didn't conducted away, and remained into the layers, and it caused grain growth.

- Effect of the scanning pattern on the grain size of samples P1 and P2:

Samples P1 (Figure 13c) and P2 (Figure 13d) were fabricated with unidirectional and bidirectional scanning direction, respectively. In these two samples, the first layer is made with 300 W, and the fifth layer is finished with 100 W. These samples are also

made with similar input parameters. According to the results in Table 5, it was found that in samples P1 and P2, the grain size decreased from the beginning to the end of samples. The grain size at the beginning of the sample is much larger, for two reasons. The first reason is that the substrate acts as a heat source [28, 29]. When the irradiation of the laser beam occurs, the substrate stored the heat on itself. Because the thermal conductivity of the steel substrate ($k=24.6$ W/m.k) is higher than that of stellite 6 ($k=14.82$ W/m.k) [30], it transfers this heat to its upper layer. This effect decreases from the beginning of the layer to the end of the layer due to the distance from the substrate. The second reason is that in these two samples, as the number of layers increases, the power per layer is reduced by 50 W. Reducing power from the first layer (300 W) to the fifth layer (100 W) reduces the temperature from the first layer to the fifth layer. This decrease in temperature causes the grains to be smaller.

On the other hand, sample P1 has smaller grains than in P2 in all three regions (beginning, center, and end of sample). This is due to a more uniform cooling rate as well as a longer time in the P1 sample. This causes the P1 sample to have a lower temperature during manufacture, resulting in smaller grain growth and smaller grain size than the P2 sample. Grain size variations at the beginning, center, and end of samples P1 and P2 are shown in Figure 13, and the trend of grain size variations in samples P1 and P2 are shown in Figure 14. According to the mentioned Figures, it is clear that the grain size has been decreased from the beginning to the end of the sample.

In all samples in 5 layers deposited LAMed wall, the heat temperature transfer effect will be reduced in the upper layers by getting away from the substrate surface, and the grain growth process will be reduced. In another way, it can be said that, the cooling rate will be higher. In Figures 13 and 14, it is shown that the top layers have a larger grain size. In addition to what has been said before, the top of the additive manufactured layers was conducted with shielding gas and air from one side. These gases have a low heat conduction coefficient, so the absorbed heat in the end layers didn't conduct away and remained into the layers, and it caused grain growth. It is also seen manufactured samples contain large columnar grains that initiate epitaxial that is because of high-temperature gradients and rapid solidification conditions [18]. Also, as confirmed in previous studies, the transition between these grain types is controlled by the thermal gradient (G) and solidification front velocity (V) at the solid-liquid interface [31]. The bottom part of each layer exhibited a columnar microstructure due to the high thermal gradient and low solidification velocity in both deposits. In contrast, the top of each layer exhibited equiaxed dendritic structure due to

the low thermal gradient and high solidification velocity at the upper part of the melt pool [32]. Furthermore, columnar crystals formed at the bottom and middle sections, and equiaxed crystals formed at the top sections, because of columnar to equiaxed transition transformation. The deposition of the upper layers during the DED process had a heat treatment effect on the lower layers. Grain coarsening occurred in the middle part by the cyclic heat treatment, and more second phases were precipitated [19]. So, it can be said that, the size of the microstructures of samples is changing with increasing the deposited layer [25]. Furthermore, with increasing the time for grain or microstructure growth, the grain size increases because of the increased thermal accumulation or decreased cooling rates [25]. As shown in fig. 14, the grain size in sample P2 is larger than P1 and in D2 is larger than D1 because of successive deposition and thermal accumulation.

- **Effect of the laser power reduction on the grain size of LAMed**

Laser power has a significant effect on the microstructure evolution of LMD formed samples [32]. As shown in Figure 14, with employing the strategy of laser power reduction from the first layer to upward, in samples P2 and P1 in comparison to D2 and D1, respectively, the grain size in all regions of deposited layer exception the beginning region of the sample (a1 and a2) became lower. This is because of applying lower power in each layer in samples P2 and P1 in comparison to D2 and D1, respectively. With decreasing the laser power in each layer, the heat produced in that layer decreases, and as a result, the grain size decrease. Previous researches also showed that the finer grain structure and coarser grain structure were generated at low laser power and high laser power, respectively [33]. And of course, increasing the laser power generally lead to a coarser grains and microstructures.

3-5. Microhardness

Microhardness of the manufactured samples was determined by a microhardness tester device in Vickers standard along the height direction of the LAMed samples. Microhardness distribution profile related to the SEM cross-section images of LAMed wall in a horizontal view is shown in Figure 13, which are measured in zones including the substrate, the first layer, the middle layer, and the end of the deposited layer along the central axis of all manufactured wall samples. The first point on the profile (zero points) represents microhardness value inside the substrate, and the last point represents microhardness value at the end zone of the sample. Also, as illustrated

in Figure 13, the height of the manufactured samples can be seen in the horizontal axis.

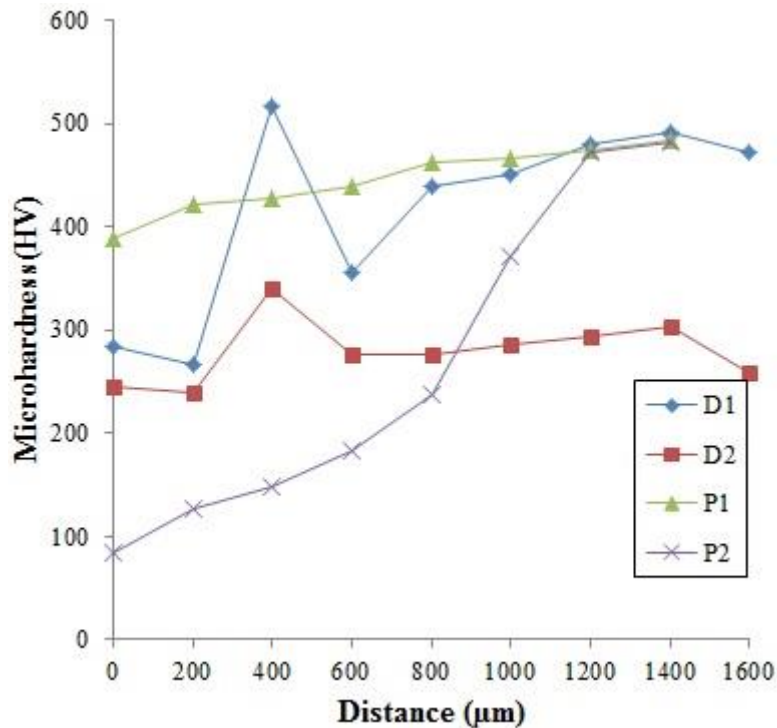


Figure 14: Microhardness distribution related to the cross-section of LAMed wall

In all the microhardness curves shown below, we find a point where the hardness has increased sharply, which is called the heat affected zone (HAZ). In fact, in this area, the steel, used as the substrate, is combined with stallite 6, which is a cobalt-based superalloy. And with the radiation of the laser beam on the steel substrate, it is possible to increase the hardness of the substrate due to the possibility of the heat treatment and alloying.

- Effect of the scanning pattern on microhardness of samples D1 and D2:

By comparing the microhardness behavior in samples D1 (unidirectional scanning pattern) and D2 (bidirectional scanning pattern), it was found that both samples have similar trends in microhardness changes. But they are different in terms of microhardness values. The difference in microhardness values of these two samples is due to differences in grain size. Sample D1 (unidirectional scanning pattern) has a lower temperature during fabrication due to its more uniform cooling rate and longer cooling time, and ultimately its grain size is smaller than sample D2 [34- 36]. The smaller grain size in an area, the more strength, and hardness the area becomes [37, 38]. Also, based on the Hall-Petch relation, equation 6 [38], it can be shown that by

decreasing the grain size, the yield strength increases, and as the yield strength increases, the material strength increases [39]. Therefore, it can be concluded that, the hardness of sample D1 is higher than that of sample D2. The curve of the microhardness changes in these two samples is showing in Figure 15.

$$\sigma_y = \sigma_0 + Kd^{-0.5} \quad (6)$$

Where σ_y is the yield strength after a change in grain size, σ_0 is the yield strength of raw material, K is the constant coefficient of the equation, and d is the average grain diameter [33].

- **Effect of the scanning pattern on microhardness of samples P1 and P2:**

Microhardness test on sample P1 (unidirectional scanning pattern) and P2 (bidirectional scanning pattern) revealed that in both samples, the hardness increased from the beginning of the sample to the end of the sample. But, these two samples are different in terms of microhardness values. The microhardness value in P1 was higher than that in P2, and also the microhardness value was less in the whole of sample P1. This hardness trend in these two samples is confirmed by the grain size in the SEM images. Generally, sample P1 has lower grain growth, and as a result of smaller grain sizes than P2, due to a more uniform cooling rate as well as longer cooling time and thus lower temperatures during manufacture. Also, the grain size in the whole of this sample is less varied. By decreasing the grain size in this sample, its hardness and strength increase. Based on the Hall-Petch relation [39], it can be shown that by reducing the grain size, the yield strength increases, and as the yield strength increases, the material strength increases [40]. Thus, the trend of microhardness changes in these two samples can be confirmed. The curve of microhardness changes for P1 and P2 is shown in Figure 15.

- **Effect of the laser power reduction on the microhardness of LAMed**

Laser power is also effective on properties of LMD formed samples [41]. As shown in Figure 15, with employing the strategy of laser power reduction from the first layer to upward, in samples P2 and P1 in comparison to D2 and D1, respectively, the microhardness values in all regions of deposited layer exception the beginning region of sample (a1 and a2) became higher. This is because of applying lower power in each layer in samples P2 and P1 in comparison to D2 and D1, respectively. With decreasing

the laser power in each layer, the heat produced in that layer decreases and the grain size decrease, and as a result, the value of microhardness increases.

In the Laser metal deposition process, with decreasing the laser power, the microhardness increase. Because, as the laser was decreased, the melt pool created on the surface of the substrate becomes smaller and the smaller the melt pool, the shorter it takes for the melt pool to cool down and as a result, the grain size decrease and finally the microhardness increase [42].

Furthermore, as mentioned in section 3.4, the re-melting and recrystallizing of the previous layer by the laser beam in adding the new layer, leads to changes in the microstructure of the interlayer as well. Also, those changes caused fluctuation in the microhardness. See Figure 15 for variation in microhardness. Also, variation in grain size is evidence in Figure 13, which confirms the trend of Figure 14.

4. Conclusion

In this paper, the effect of scanning pattern in fiber laser additive manufacturing process of stellite 6 powders was investigated. Results from both microstructural, dimensional, and mechanical characterization of the samples indicate that, the higher microhardness, lower distortion, higher stability, and lower grain size can be obtained when using a unidirectional scanning pattern. Generally, according to the experiments, the following results can be drawn:

- 1- For more stability will be generated when the unidirectional scanning pattern was used.
- 2- The grain size in the beginning and the end of the LAMed wall samples are larger than the sample's center, which is related to the temperature inside the melt pool in the deposition process. The higher melt pool temperature was led to a bigger grain size.
- 3- The trend of the microhardness changes is in the reverse regime of the grain size. The smaller the grain size led to the higher microhardness. The microhardness in the center of the sample was higher than the beginning and end of the sample.
- 4- The laser power reduction is also effective on grain size and microhardness of samples. It was shown that with employing strategy of power reduction from the first layer to upward in comparison to constant laser power strategy, the grain size and microhardness became lower and larger, respectively.

References:

- [1]. Z. Wang, J. Zhao, Y. Zhao, H. Zhang, F. Shi, (2017), Microstructure and microhardness of Laser Metal Deposition Shaping K465/Stellite-6 laminated material, *Metals Journal*, 7, 512.
- [2]. R.Liu, Z.Wang, T.Sparks, F.Liou, J.Newkirk, (2017), *Laser Additive Manufacturing: Materials, Design, Technologies, and Applications*, Aerospace applications of laser additive manufacturing, Woodhead Publishing, 351-371.
- [3]. T. DebRoy, L. Wei, J.S. Zuback, T. Mukherjee, J.W. Elmer, J.O. Milewski, A.M.Beese, A.Wilson-Heid, A.De, W.Zhang, (2018), Additive manufacturing of metallic components – Process, structure and properties, *Progress in Materials Science*, vol. 92, 112-224.
- [4]. A. Mostafaei, P. Rodriguez De Vecchis, M.J. Buckenmeyer, S. R. Wasule, B. N. Brown, M. Chmielus, (2019), Microstructural evolution and resulting properties of differently sintered and heat-treated binder jet 3D printed Stellite 6, *Materials Science & Engineering C*, vol. 102, 276-288.
- [5]. E. T. Akinlabi, S.A. Akinlabi, (2016), *Advanced coating: Laser Metal Deposition of Aluminium powder on Titanium Substrate*, *Proceedings of the World Congress on Engineering*, vol. II.
- [6]. Z. Gan, G. Yu, X. He, S. Li, (2017), Numerical simulation of thermal behavior and multicomponent mass transfer in direct laser deposition of Co-based alloy on steel, *International Journal of Heat and Mass Transfer*, 104, 28–38.
- [7]. H. Gu, L.Li, (2019), Computational fluid dynamic simulation of gravity and pressure effects in laser metal deposition for potential additive manufacturing in space, *International Journal of Heat and Mass Transfer*, 140, 51–65.
- [8]. S.M. Thompson, L. Bian, N. Shamsaei, A. Yadollahi, (2015), An Overview of Direct Laser Deposition for Additive Manufacturing Part I: Transport Phenomena, Modeling, and Diagnostics, *Additive Manufacturing*, 8, 36-62.
- [9]. N. Shamsaeia, A. Yadollahia, L. Bianc, S. M. Thompsona, (2015), An overview of Direct Laser Deposition for additive manufacturing; Part II: Mechanical behavior, process parameter optimization and control, *Additive Manufacturing*, 8, 12-35.
- [10]. W. Oh, Y. Son, D. S. Shim1, (2019), Effect of In-Situ Post Heating on Repairing STS316L Built by Laser Powder Bed Fusion Using Direct Energy Deposition, *Korean J. Met. Mater*: 57(8), 543-553.
- [11]. H. Freibe, P. Khazan, M. Stroth, H. Köhler, (2015), Properties of large 3D parts made from Stellite 21 through direct powder deposition, *Lasers in Manufacturing Conference*.
- [12]. G.J. Marshall, W. J.Young, S. M.Thompson, N. Shamsaei, S. Daniewicz, S. Shao, (2016), Understanding the microstructure formation of Ti-6Al-4V during direct laser deposition via in-situ thermal monitoring, *Jom*, 68(3), 778-790.
- [13]. E. Bagci, S. Aykut, (2006), A study of Taguchi optimization method for identifying optimum surface roughness in CNC face milling of cobalt-based alloy (stellite 6), *The International Journal of Advanced Manufacturing Technology*, Vol. 29, 940–947.
- [14]. J. Foster, C. Cullen, S Fitzpatrick, G Payne, L. Hall, J. Marashi, (2019), Remanufacture of hot forging tools and dies using laser metal deposition with powder and a hard-facing alloy Stellite 21, *Remanufacturing*, (9),189–203.

- [15]. M.T. Dalae, L. Gloor, Ch. Leinenbach, K. Wegener, (2020), Experimental and numerical study of the influence of induction heating process on build rates Induction Heating-assisted laser Direct Metal Deposition (IH-DMD), *Surface and Coatings Technology*, Vol. 384, 125275.
- [16]. F. Caiazza, A. Caggiano, (2018), Laser Direct Metal Deposition of 2024 Al Alloy: Trace Geometry Prediction via Machine Learning, *Materials*, 11, 444.
- [17]. O. Zinovieva, A. Zinoviev, V. Ploshikhin, (2018), Three-dimensional modeling of the microstructure evolution during metal additive manufacturing, *Computational Materials Science*, vol. 141, 207–220
- [18]. K. Shah, A. J. Pinkerton, A. Salman, L. Li, (2010), Effects of melt pool variables and process parameters in laser direct metal deposition of aerospace alloys, *Materials and Manufacturing Processes*, 12, 1372-1380.
- [19]. T.T. Roehling, Sh. S.Q.Wu, S. A.Khairallah, J. D.Roehling, S. StefanSoezeri, M. F.Crumb, M. J.Mathew, (2017), Modulating laser intensity profile ellipticity for microstructural control during metal additive manufacturing, *Acta Materialia*, 128, 197-206.
- [20]. T. Gu, B. Chen, C. Tan, J. Feng, (2019), Microstructure evolution and mechanical properties of laser additive manufacturing of high strength Al-Cu-Mg alloy, *Optics and Laser Technology*, 112, 140–150.
- [21]. M. Moradi, A. Ashoori, A. Hasani, (2020), Additive Manufacturing of Stellite 6 Superalloy by Direct Laser Metal Deposition – Part 1: Effects of Laser Power and Focal Plane Position, *Optics and laser technology*, Article in Press. <https://doi.org/10.1016/j.optlastec.2020.106328>
- [22]. K. Zhang, X. Shang, W. Liu, (2009), Study on Scanning Pattern during Laser Metal Deposition Shaping, *Second International Conference on Intelligent Computation Technology and Automation*.
- [23]. A. Kudzal, B. McWilliams, C. Hofmeister, F. Kellogg, J. Yu, J. Taggart-Scarff, J. Liang, (2017), Effect of scan pattern on the microstructure and mechanical properties of Powder Bed Fusion additive manufactured 17-4 stainless steel, *Materials & Design*, Vol. 133, 205-215.
- [24]. Nick Tepylo, Xiao Huang, and Prakash C. Patnaik, (2019), Laser-Based Additive Manufacturing Technologies for Aerospace Applications, *Advanced engineering materials*, vol. 21, Issue 11, 1900617.
- [25]. X. Zhao, S. Dong, S. Yan, X. Liu, Y. Liu, D. Xia, Y. Lv, P. He, B. Xu, H. Han, (2020), The effect of different scanning strategies on microstructural evolution to 24CrNiMo alloy steel during direct laser deposition, *Materials science and engineering*, Vol. 771, 138557.
- [26]. B. Ren, M. Zhang, C. Chen, X. Wang, T. Zou, Z. Hu, (2017), Effect of heat treatment on microstructure and mechanical properties of stellite 12 fabricated by Laser additive manufacturing, *Materials Engineering and Performance*, 26(11), 5404-5413.
- [27] American society for testing and materials (ASTM), (2004), E112 Standard Test Methods for Determining Average Grain Size.
- [28]. M. Moradi, M. Ghoreishi, J. Frostevarg, A. F. Kaplan, (2013), An investigation on stability of laser hybrid arc welding, *Optics and Lasers in Engineering*, 51(4), 481-487.
- [29]. X. Zhan, C. Qi, Z. Gao, D. Tian, Z. Wang, (2019), The influence of heat input on microstructure and porosity during laser cladding of Invar alloy, *Optics & Laser Technology*, 113, 453-461.
- [30]. M. Moradi, M. Karami Moghadam, (2019), High power diode laser surface hardening of AISI 4130; statistical modeling and optimization, *Optics & Laser Technology*, 111, 554-570.

- [31]. Th. M. Rodgers, J. D. Madison, V. Tikare, (2017), Simulation of metal additive manufacturing microstructures using kinetic Monte Carlo, *Computational Materials Science*, 135, 78–89.
- [32]. A. Singh, (2017), Additive Manufacturing of Al 4047 And Al 7050 Alloys Using Direct Laser Metal Deposition Process, Ph.D. thesis, Wayne State University.
- [33]. A.A. Adeyemi, E. T. Akinlabi, R. M. Mahamood, K. O. Sanusi, S. Pityana , M. Tlotleng, (2017), Influence of laser power on microstructure of laser metal deposited 17-4 ph stainless steel, *IOP Conference Series: Materials Science and Engineering*, Vol. 225.
- [34]. D. Schnubel, M. Horstmann, V. Ventzke, S. Riekehr, P. Staron, T. Fischer, N. Huber, (2012), Retardation of fatigue crack growth in aircraft aluminium alloys via laser heating–Experimental proof of concept, *Materials Science and Engineering: A*, 546, 8-14.
- [35]. A.R. A. Dezfoli, W. Hwang, W. Huang, T. Tsai, (2017), Determination and controlling of grain structure of metals after laser incidence: Theoretical approach, *Scientific reports*, 7, 41527.
- [36]. D. Yao, J.K. Shang, (1996), Effect of cooling rate on interfacial fatigue-crack growth in Sn-Pb solder joints, *IEEE Transactions on Components, Packaging, and Manufacturing Technology: Part B*, 19(1), 154-165.
- [37]. P. Asghari-Rad, P. Sathiyamoorthi, J. Wung Bae, J. Moon, J. M. Park, A. Zargaran, H. S. Kim, (2019), Effect of grain size on the tensile behavior of V10Cr15Mn5Fe35Co10Ni25 high entropy alloy, *Materials Science and Engineering: A*, 744, 610-617.
- [38]. S. Kanga, J. Junga, M. Kang, W. Woo, Y. Lee, (2016), The effects of grain size on yielding, strain hardening, and mechanical twinning in Fe–18Mn–0.6 C–1.5 Al twinning-induced plasticity steel *Journal of Materials Science and Engineering: A*, 652, 212-220.
- [39]. E. Hall, (1951), The deformation and aging of mild steel: III discussion of results, *Proceedings of the Physical Society, Section B* 64, 747-753.
- [40]. M. Lashani Zand, B. Niroumand, A. Maleki, (2019), Determination of the Modified Hall-Petch Equation Constants and the Relationship Between the Microstructure and Mechanical Properties of AS7U3G Alloy, *Advanced Materials in Engineering*, 37(4), 91-100.
- [41]. X. Kang, S. Dong, H. Wang, S. Yan, X. Liu, B. Xu, (2020), Effect of Laser Power on Gradient Microstructure of Low-Alloy Steel Built by Laser Melting Deposition, *Materials letter*, Vol. 262, 127073.
- [42]. R. M. Mahamood, E. T. Akinlabi, S. Akinlabi, (2015), Laser power and Scanning Speed Influence on the Mechanical Property of Laser Metal Deposited Titanium-Alloy, *Lasers in Manufacturing and Materials Processing* (2) , 43–55.